The porcine corticospinal decussation: A combined neuronal tracing and tractography study

Bech, Johannes; Glud, Andreas N.; Sangill, Ryan; Petersen, Mikkel; Frandsen, Jesper; Orlowski, Dariusz; West, Mark J.; Pedersen, Michael; Sørensen, Jens Christian H.; Dyrby, Tim Bjørn

Total number of authors:
11

Published in:
Brain Research Bulletin

Link to article, DOI:
10.1016/j.brainresbull.2018.08.004

Publication date:
2018

Document Version
Publisher's PDF, also known as Version of record

Brain Research Bulletin 142 (2018) 253–262

Contents lists available at ScienceDirect

Brain Research Bulletin

journal homepage: www.elsevier.com/locate/brainresbull

Research report

The porcine corticospinal decussation: A combined neuronal tracing and tractography study

Johannes Bech[a,*], Andreas N. Glud[a], Ryan Sangill[b], Mikkel Petersen[b], Jesper Frandsen[b], Dariusz Orlowski[a], Mark J. West[a], Michael Pedersen[c], Jens Christian H. Sørensen[a], Tim B. Dyrby[d,e], Carsten R. Bjarkam[f]

[a] CENSE, Dept. of Neurosurgery, Aarhus University Hospital, & Department of Clinical Medicine, Aarhus University, DK-8000 Aarhus, Denmark
[b] CFIN, Department of Clinical Medicine, Aarhus University, DK-8000 Aarhus, Denmark
[c] Comparative Medicine Lab, Department of Clinical Medicine, Aarhus University, DK-8200 Aarhus N, Denmark
[d] Danish Research Centre for Magnetic Resonance, Center for Functional and Diagnostic Imaging and Research, Copenhagen University Hospital Hvidovre, DK-2650 Hvidovre, Denmark
[e] Dept. of Applied Mathematics and Computer Science, Technical University of Denmark, DK-2800 Kongens Lyngby, Denmark
[f] Dept. of Neurosurgery, Department of Clinical Medicine, Aalborg University Hospital, DK-9100 Aalborg, Denmark

ARTICLE INFO

Keywords:
Corticospinal decussation
Göttingen minipig
Neuronal tracing
Pyramidal tract
Stereology
Tractography

ABSTRACT

Background: Pigs and minipigs are increasingly used as non-primate large animal models for preclinical research on nervous system disorders resulting in motor dysfunction. Knowledge of the minipig pyramidal tract is therefore essential to support such models.

Aim and methods: This study used 5 female Göttingen minipigs aging 11–15 months. The Göttingen minipig corticospinal tract was investigated, in the same animals, with in vivo neuronal tracing and with postmortem diffusion weighted MRI tractography to provide a thorough insight in the encephalic distribution of this primary motor pathway and its decussation at the craniocervical junction.

Results: The two methods similarly outlined the course of the pyramidal tract from its origin in the motor cortex down through the internal capsule to the craniocervical junction, where both methods displayed an axonal crossover at the pyramid decussation. The degree of crossover was quantified with unbiased stereology, where 81–93% of the traced corticospinal fibers crossed to the contralateral spinal cord. Accordingly, in the upper cervical spinal cord the corticospinal tract is primarily distributed in the contralateral lateral funiculus and in close relation to the gray matter, wherein some direct terminations on large ventral column gray matter neurons could be identified.

Discussion: The combination of neuronal tracing and tractography exploited the strengths of the respective methods to gain a better understanding of the encephalic distribution and craniocervical decussation of the Göttingen minipig corticospinal tract. Moreover, a quantification of the crossing fibers was obtained from the tracing data, which was not possible with tractography. Our data indicate that the porcine corticospinal system is quite lateralized down to the investigated upper cervical levels. However, further elucidation of this point will require a full examination of the corticospinal tracing pattern into the caudal spinal cord combined with an analysis of the direct versus indirect termination pattern on the lower motor neurons.

1. Introduction

Pigs and minipigs (sus scrofa) have been increasingly used as non-primate large research animals for preclinical research on nervous system disorders resulting in motor dysfunction (Bjarkam et al., 2008; Christensen et al., 2018; Cumming et al., 2001; Dolezalova et al., 2014; Glud et al., 2011; Nielsen et al., 2016; Schubert et al., 2016; Tanaka et al., 2008), as they have a large gyrencephalic brain relative to their body size permitting the use of conventional neurosurgical equipment and clinical scanners (Bjarkam et al., 2008; Glud et al., 2010; Lind et al., 2007). Moreover, pigs are easy to handle, and their anatomy and physiology closely resembles that of humans (Fang et al., 2012). Also, they have both economical and ethical advantages compared to the use of non-human primates (Bjarkam et al., 2009; Glud et al., 2010).

* Corresponding author at: Aarhus University Hospital, Dept. of Neurosurgery, Nørrebrogade 44, Build. 10, 5., DK-8000 Aarhus C, Denmark.
E-mail address: jb@clin.au.dk (J. Bech).

https://doi.org/10.1016/j.brainresbull.2018.08.004
Received 26 March 2018; Received in revised form 28 July 2018; Accepted 2 August 2018
Available online 04 August 2018
0361-9230/

However, the neuroanatomical knowledge of the porcine corticospinal tract (CST) is sparse, as it generally has been expected that this fiber system in hoofed animals (ungulates) was less developed reflecting the lacking ability for skilled precision movements of the distal extremities (Lassek, 1942). This belief was supported by an anatomical study of the landrace pig pyramidal tract indicating that corticospinal fibers were not seen caudal to the first cervical metamere (Palmieri et al., 1986). More recent studies using fMRI (Fang et al., 2005), muscle motor evoked potentials (Tanaka et al., 2008), and neuronal tracing (Leonard et al., 2017) have, however, questioned the classical view on the porcine corticospinal system. Thus, passive movement of the pig hind limb will result in activation of pig cortical motor areas (Fang et al., 2005), just as lesion of the internal capsule will abolish limb muscle motor evoked potentials contralateral to the lesion (Tanaka et al., 2008). Neuronal tracing from the pig motor cortex (MC) have likewise demonstrated that the pig corticospinal tract can be seen in the cervical spinal cord, where it is located in the lateral fiber column similar to humans, but in contrast to the position of the rodent corticospinal tract in the dorsal column (Leonard et al., 2017). It is, however, noteworthy that the CST is not demonstrated directly in the former two studies (Fang et al., 2005; Tanaka et al., 2008), while the study by Leonard et al. (Leonard et al., 2017) do not mention the degree of pyramidal decussation and neither indicate whether their demonstrated unilateral cervical CST is located ipsilateral or contralateral to the tracer injection in the motor cortex.

In order to understand white matter tracts, neuronal tracing has been used for years to investigate neuronal connections and is currently the gold standard (Dyrby et al., 2007; Vercelli et al., 2000). Biotinylated dextran amine (BDA) has been successfully used for anterograde neuronal tracing across animal species (Brandt and Apkarian, 1992; Reiner et al., 2000; Veenman et al., 1992), e.g. for tract tracing of the canine CST (Han et al., 2012). The invasive nature of this technique, however, limits its applicability. On the other hand, tractography derived from diffusion weighted MRI is a non-invasive method that can be performed both in and *ex vivo* to study neuronal connections (Anaya Garcia et al., 2015; Dyrby et al., 2011) in animals as well as in humans. Contrary to neuronal tracing, tractography is not a labelling of individual axons, but the imaging technique is based on the anisotropic water diffusion inside and between the axons. There have been obstacles due to factors as low spatial resolution, low signal-to-noise ratio and complex white matter regions with multiple crossing fibers (Calabrese et al., 2015; Tournier et al., 2004), where the latter has been described to cause problems with both false positives and false negatives (Tournier et al., 2012). To handle such complex local microanatomy, local crossing fiber models can be used (Behrens et al., 2007).

This study aims, accordingly, to describe the Göttingen minipig corticospinal decussation combining, in the same animal, neuronal tracing and tractography. Additionally, the laterality of the CST will be quantitatively assessed by the use of unbiased stereology (West, 2012a).

2. Materials and methods

2.1. Pilot study

The neuronal tracing procedure, techniques and survival time was determined based on a pilot study in rats and existing literature (Lazarov, 2013; Reiner et al., 2000).

2.2. Main study

2.2.1. Animals

5 female Göttingen minipigs (*Ellegaard Göttingen Minipigs, Dalmose, DK),* JBG-1 to JBG-5, aging 11–15 months and weighing 22.6–28.0 kg were used in this study as approved by the Danish National Council of Animal Research Ethics (protocol number 2015-15-0201-00965).

2.2.2. Materials

BDA tracing solution was freshly made prior to each injection using lyophilized BDA powder (NeuroTrace™ BDA-10.000 Neuronal Tracer Kit, ThermoFischer, Waltham, MA, USA) dissolved in 0.01 M phosphate buffered saline (PBS) with pH 7.4 yielding a 10% BDA solution.

2.2.3. Surgical preparation and neuronal tracer injection

Animals were sedated with 10 ml sedative mixture (6 ml midazolam 5 mg/mL, 4 ml ketamine 25 mg/mL, i.m.). Intravascular access was obtained through cannulation of an ear vein and animals were further sedated before being intubated as previously described (Ettrup et al., 2011) permitting isoflurane anaesthesia and respirator ventilation. Animals received buprenorphin (*Temgesic®*) analgesic and antibiotic prophylaxis bolus (1.5 g *Cefuroxim "Fresenius Kabi"*) and were placed in a MRI-compatible headframe providing stability and attachment of stereotaxic equipment (Bjarkam et al., 2004). A midline incision was made subsequent to a subcutaneous local anaesthetic injection and a fiducial marker was inserted in a skull burr hole. Anatomical scans for fiducial marker visualization and stereotaxic planning were then acquired on a 3 T Siemens Magnetom Trio MR scanner (Tim Trio) using a Turbo Flash 3D T1-weighted sequence with slice thickness 1 mm, voxel size $1 \times 1 \times 1\ mm^3$, 176 slices, FOV = 256, TR = 2420 ms, TE = 3.7 ms, 2 averages, TI = 960 ms, and flip angle = 9°. During the scan animals were placed in a prone position on a 24 element spine matrix coil with a 6 element body matrix coil on top of the stereotaxic frame.

The position of the Göttingen minipig motor cortex known from a previous study (Bjarkam et al., 2017a) could now be estimated in relation to the MRI-visualized skull fiducial marker (Glud et al., 2017) and a burr hole craniotomy was then placed over the estimated position of the right motor cortex. The dura was opened with a dura knife revealing the dorsal surface anatomy of the right hemisphere. It was now possible, as indicated on Fig. 1, to identify the longitudinal cerebral fissure, and the ansate, the cruciate and the coronal sulci, which delineate the motor cortex (Bjarkam et al., 2017a). The BDA solution was slowly pressure injected (0.1 µL/min) using a 10 µL Hamilton microsyringe placed in a manual micromanipulator system. To ensure a sufficient amount of traced neurons from the exposed brain surface, the right motor cortex was injected at three separate sites separated by 1 mm in the anterior-posterior direction at three depths (surface −3 mm, surface −2 mm, and surface −1 mm) yielding the same total dose of 4.5 µL tracer in all animals and covering an injection area for each animal as indicated on Fig. 1. After each injection, the syringe was left for 5 min to prevent reflux of the tracer along the needle track (Nance and Burns, 1990). The dura was replaced and covered with BioGlue® (*CryoLife, Kennesaw, Georgia, US*) and the scalp re-sutured.

2.2.4. Tissue fixation

After 26–31 days, animals were euthanized by an intra-cardial pentobarbital overdose after sedation. The brain was trans-cardially perfusion fixated with 5 l phosphate buffered paraformaldehyde (PFA) in a 4% solution (pH 7.4) using a pressurized container with a catheter tip placed in the ascending aorta through the left ventricle (Ettrup et al., 2011). The fixated brain and the upper spinal cord were removed subsequent to surgical skull removal and laminectomy (Bjarkam et al., 2017b). The cortical injection area was labeled with red tissue staining (India Ink®) through the surgical dura opening. The removed brains were initially placed in 4% PFA solution until at least a week prior to ex vivo DWI scanning where they were transferred to a neutral 0.01 M PBS solution.

2.2.5. Diffusion weighted magnetic resonance imaging

Ex vivo DWI was acquired on a 4.7T Agilent MR scanner at Danish Research Centre for Magnetic Resonance (DRCMR). The preparation of the brains for ex vivo imaging used the procedure previously described by Dyrby et al. (Dyrby et al., 2011) allowing a long-time imaging protocol without artefacts from respiration movements and influence of

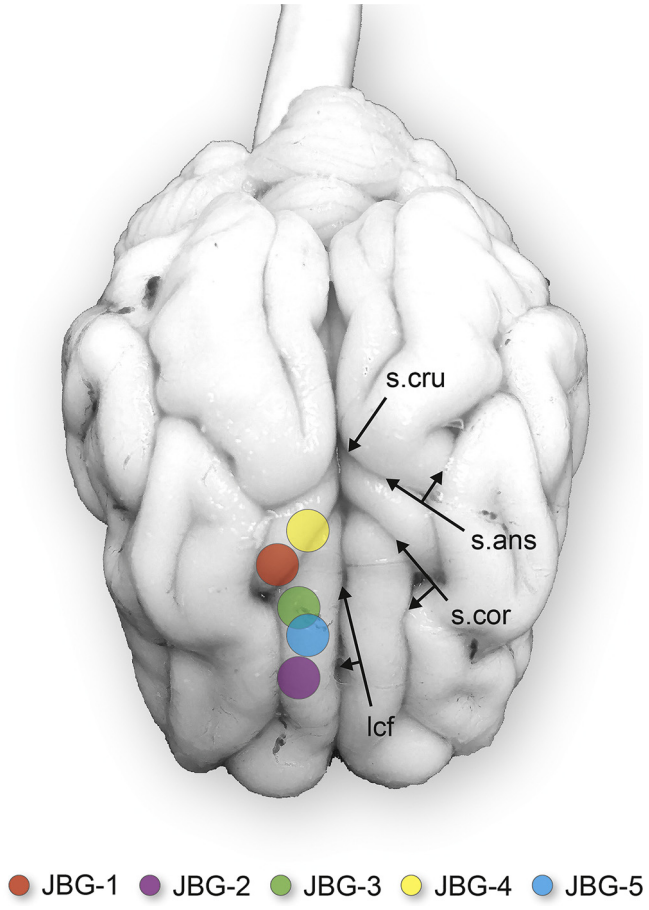

Fig. 1. Schematic figure with approximated overview of the tracer-injected areas. Areas were determined from the surface staining of individual brains merged on a single brain surface. s. ans, ansate sulcus; s. cru, cruciate sulcus; s. cor, coronal sulcus; lcf, longitudinal cerebral fissure.

air located in the overlying pneumatized frontal sinuses. Thus, the spinal cord was folded above the cortex supported by gauze and wrapped in Micropore™ tape to mechanically stabilize the position of the tissue during scanning. Before the actual scanning session was started, dummy scans of more than six hours was acquired to ensure that no short-term instabilities was introduced in the DWI dataset (Dyrby et al., 2011). Four brains were scanned (JBG-1/3/4/5). JBG-1 was later excluded since perfusion difficulties were seen to have yielded noise on the DWI scans. Scans were made using a pulsed-gradient spin-echo sequence (PGSE) with single line readout. A DWI data set included nine b = 0 s/mm^2 and a b-value of 6500 s/mm^2 (δ = 7 ms, Δ = 20 ms, Gradient strength = 320 m T/m) acquired in 128 non-collinear directions (Jones, 2004). Voxel size was 0.5 × 0.5 × 0.5 mm^3, and 105 slices ensured whole brain coverage. TR = 7200 ms, TE = 35 ms. Scanning time was approximately 48 h per session.

2.2.6. Tissue handling

After ex vivo diffusion MRI scanning, the brain and rostral cervical spinal cord down to C3 were retrieved (Bjarkam et al., 2017b), embedded in HistOmer® alginate, and sliced in 1.5–2 cm thick coronal slabs (Bjarkam et al., 2001). Subsequently slabs were placed in a 30% sucrose solution until the tissue had sunk. The injected hemisphere was labeled using red tissue staining and Bouin's fixative for histological orientation purposes. The slabs were frozen in liquid isopentane cooled by dry ice and freeze-cut in 30 µm thick coronal sections on a cryostat before being placed in PBS solution. All slabs were cut in series so that every 10th section was kept and the rest discarded except the slab containing the pyramidal decussation where every 5th section was kept.

2.2.7. Histology

The sections were rinsed with phosphate buffer before quenching with 10% H_2O_2 and 3% methanol phosphate buffer solution to knock out endogenous peroxidase. Then the tissue was rinsed, pre-incubated for 30 min in bovine serum albumin and placed 90 min in avidin-biotin-peroxidase complex solution (*VECTASTAIN® Elite ABC kit, Vector Laboratories, Burlingame, CA, US)*, before it was rinsed and placed in a DAB solution (Kem-En-Tec Nordic A/S, Taastrup, DK) for 7 min for BDA visualization. Sections were mounted on gelatin-coated glass slides and air-dried before being immersed in distilled water and counterstained in toluidine blue for 5 min. Finally, the mounted sections were dehydrated with ethanol, placed in xylene, and protected by a cover glass.

2.2.8. Stereology

Of the five animals in the study one (JBG-2) was excluded for stereological analysis since the injections were found not to be in the motor cortex after histological evaluation of the injection site. The number of traced fibers was counted under a Zeiss Axioplan 2 microscope with attached video camera using a 2D fractionator method in Stereo Investigator® software (*MBF Bioscience, Williston, VT, US*). The most caudal brainstem section yet rostral to the pyramidal decussation and, likewise, the most rostral cervical spinal cord section caudal to the pyramidal decussation were chosen for stereologic fiber counting with visible crossing fibers in the midline as exclusion criteria to avoid bias (see also Fig. 3). The ipsilateral pyramid of the cranial sections was manually defined and analyzed using a x60 lens with digitally superimposed 60 × 60 µm counting frames sized in a 240 × 240 µm grid. On caudal sections, both entire halves of the spinal cord were analyzed, respectively, using a ×20 lens, 200 × 200 µm counting frames on a 400 × 400 µm grid. Cortical injection volumes were estimated using the Cavalieri principle (West, 2012b). Injection areas were manually defined and calculated using Stereo Investigator software on a series of neighboring sections with known distance.

2.2.9. Tractography

Tractography was performed with MRtrix 3 software (http://www.mrtrix.org) (Tournier et al., 2012). Using FSL software (http://fsl.fmrib.ox.ac.uk/fsl/fslwiki/FSL) (Jenkinson et al., 2012), a brain mask was made by drawing a ROI on the b0 image in 'fslview' to confine all analyses to the brain tissue. In MRtrix 3 software we used a multi-fiber-reconstruction method, i.e. constrained spherical deconvolution (Tournier et al., 2007, 2004). Tractography was performed with the probabilistic algorithm, iFOD2 (Tournier et al., 2010). To adjust to the *ex vivo* data set, the step-length for drawing streamlines, the angle between successive steps, and the FA cut off value were changed from standard settings (Table 1). A whole-brain tractography was made using the entire brain mask for streamline seeding to provide a general overview of white matter anatomy including a gross anatomical overview of the crossing fibers at the pyramid decussation, which is not possible with neuronal tracing. Subsequent CST tractography was made using manually drawn regions of interest (ROIs). ROIs were made in the spatial planes perpendicular to the presumed direction of CST fibers by combining knowledge from the neuronal tracing data, a priori neuroanatomical knowledge, and fiber orientation distribution (FOD) glyphs (Fig. 5). In MRtrix 3 software the white matter constituting the internal capsule was drawn in the axial plane to be used as seeding ROI (see Fig. 5). Similarly, an ipsilateral MC ROI in the axial plane and ipsilateral ventral brainstem ROI in the coronal plane were drawn in a reproducible manner. These ROIs were used as waypoints, i.e. inclusion ROIs. Contrarily, the corpus callosum was defined as exclusion ROI to avoid interhemispheric streamline connections in order to visualize direct projections of the CST. Streamlines were quantified using 'tckedit' in MRtrix 3 by means of three inclusion ROIs that selected and counted the number of streamlines located, respectively, before the pyramidal crossing in the ipsilateral brainstem, in the ipsilateral spinal half, and in the contralateral spinal half. The two "spinal half" ROIs

Table 1
Listed above are the b values and the specific parameters used in the tractography in the respective animals. Parameters are subdivided into "whole" brain tractography and ICE-T "CST" tractography columns. Also note the ratio of "generated versus selected streamlines", which is indirectly related to the probability of such an existing tract. Std. is standard settings with cutoff at 0.1, angle at 90° × (step size / voxel size), and step size at (0.5 × voxel size). The last column is the final number of selected streamlines remaining after "tckedit" removal of false positives.

Animal No.	b value s/mm^2	Streamlines number ratio generated/ selected		Cutoff value		Angle degrees		Step size mm		Streamlines after tckedit
		Whole	*CST*	*Whole*	*CST*	*Whole*	*CST*	*Whole*	*CST*	*CST*
JBG-3	6500	1,515,020/1,000,000	10,000/8,969	0.12	0.3	Std.	20	Std.	0.0625	8537
JBG-4	6500	1,932,473/1,000,000	10,000/8,585	0.2	0.3	Std.	20	Std.	0.0625	8383
JBG-5	6500	2,000,000/1,318,260	10,000/8,925	0.25	0.3	20	20	0.0625	0.0625	8301

were made caudal to visible crossing streamlines to avoid bias in the quantification. This permitted a streamline count in these regions for comparison. Subsequently, we used an ICE-T approach that can better segment the shape of the CST by using a region growing method creating a new seed (Liptrot et al., 2014). This was done using 'tckmap' in MRtrix 3 to create a binary seeding ROI representing the CST, which was then used as seed for the final tractography with the corpus callosum and posterior commissure as exclusion ROIs. With knowledge from the neuronal tracing data, this tractography had readily recognizable smaller groups of false positive streamlines emerging from complex white matter regions as the centrum semiovale. These were edited with 'tckedit' by using reproducible exclusion ROIs in the parietal lobe (coronal and sagittal plane), the external capsule, and the contralateral ventral upper brainstem to better represent the CST.

3. Results

3.1. Neuronal tracing

The animals were injected at different cortical areas previously described as representing the minipig motor cortex (Bjarkam et al., 2017a; Palmieri et al., 1986). A visual overview was obtained combining the surface staining representing the injection sites of the respective brains. Accordingly, the surface stained areas were merged and displayed on one brain surface to evaluate the extent and degree of motor cortical representation in the tracing data (Fig. 1).

The neuronally traced cortical areas were histologically analyzed across animals to evaluate and confirm motor cortical targeting with emphasis on cortical cytoarchitecture and section topography. The overall topography and predominance of the pyramid cell layers III and V as well as large pyramid cells in layer V were thus considered indicative of the minipig motor cortex (primary motor + premotor cortex) and hence a correctly placed injection (Bjarkam et al., 2017a). This was present in four animals (JBG-1/3/4/5) (Fig. 2), whereas the pyramidal cells of layer V in the remaining animal (JBG-2) seemed somewhat smaller as is known to be the case for the prefrontal cortex, which is more anteriorly located than the minipig motor cortex (Bjarkam et al., 2017a).

The axonal projections of traced motor cortical neurons descended in the gyral white matter before turning around the lateral ventricle to the centrum semiovale and further into the internal capsule. Reciprocal connections to previously described thalamic nuclei were evident (Bjarkam et al., 2017a; Solnitzky, 1938). In four animals (JBG-1/3/4/5) such connections were found in the ventroanterior and/or ventrolateral nuclei (VA-VL) involved in motor function, whereas the remaining animal (JBG-2) had connections to the mediodorsal thalamic nucleus (MD).

In all analyzed brains, except JBG-2, the motor cortical neuron axons projected caudally in the ipsilateral ventral brainstem pyramid forming the CST (Fig. 3A). In the medulla oblongata, the fibers gradually turned dorsomedial before the vast majority of fibers crossed the midline at the pyramid decussation and continued caudally in the contralateral spinal cord, predominantly in the lateral funiculus (Fig. 3D + E). Moreover, some fibers converged towards the dorsal horn of the spinal gray matter. The uncrossed fibers displayed a similar course predominantly residing within the lateral funiculus (Fig. 3D). Some uncrossed fibers were, however, seen in proximity to the median ventral fissure in one animal (JBG-3). In the rostral cervical spinal cord some CST terminals were noted in close contact to large neuronal cell bodies of the ventral horn gray matter (Fig. 3F). Findings are summarized in Fig. 3 and Table 2.

3.2. Stereology

The laterality of the CST was assessed by quantifying the crossed versus uncrossed fibers. From this quantification, it was apparent that a majority ranging from 81 to 93% of the traced corticospinal fibers crossed to the contralateral spinal cord. One animal deviated slightly (81%) from the others due to the presence of the previously described ventral group of uncrossed fibers. There were differences in the total amount of traced fibers, which could, however, not be ascribed to different cortical volumes of injected tracer evaluated by Cavalieri volume estimation. The precision of the volume estimates was below the accepted 0.1 value of observed coefficient of error (OCE). See Table 3.

3.3. Tractography

Initially, whole brain tractography was made to provide a detailed overview of the white matter anatomy. This displayed a consistent directional shift of streamlines at the pyramid decussation indicating a crossover of corticospinal fibers in animals JBG-3/4/5 (Fig. 4).

The corticospinal tractography outlined the course of the tract from the motor cortex until the crossing fibers entered the spinal cord gray matter, where the low degree of anisotropy caused the streamlines to either terminate or continue in what seems an anatomically implausible manner. Like the neuronally traced fibers, streamlines descended from the motor cortex to take a sharp turn around the lateral ventricle before traversing down the internal capsule. The position in the ventral brainstem pyramid was, likewise, comparable with tracing data. The position of fiber crossover at the pyramid decussation correlated well with the tracing data, whereas the crossover percentage of quantified streamlines varied and was not in accordance with the tracing data. Furthermore, this quantification outlines the large number of streamlines terminating immediately after crossing, which correspond to the low total number of streamlines below crossing. See Table 4. Few false positive streamlines identified using the tracing data were seen in immediate relation to complex white matter areas, i.e. the centrum semiovale and brainstem. The ratio of generated versus selected streamlines was, however, questionable suggesting a somewhat low probability of the displayed tract since only few streamlines were able to fulfill the defined criteria.

Since the used tractography algorithm was probabilistic and the investigated tract had a long course, we subsequently used a previously described ICE-T wrapper to address issues of path-length dependency confounds (Liptrot et al., 2014). This method provided a far better ratio between generated and selected streamlines, whereas the course of the

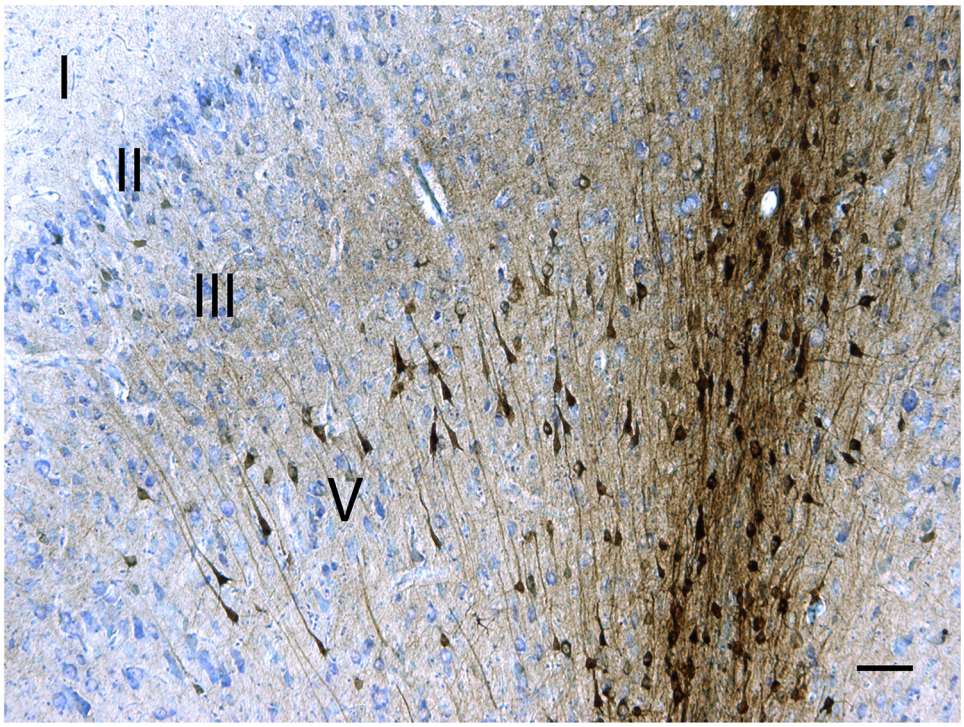

Fig. 2. Injected cortical area of JBG-4 with marked cytoarchitectonic layers I, II, III and V. The cytoarchitecture consists of a dominant layer III and V. Note the large tracer stained pyramidal cells in layer V. The above mentioned are typical features of the minipig motor cortex. The needle track is seen to the right. Counterstaining with toluidine blue. Scale bar 100 μm. (For interpretation of the references to color in this figure legend, the reader is referred to the web version of this article.)

CST (Fig. 5) was similar with the exception of slightly more false positive streamlines. Such were emerging from the previously mentioned complex white matter areas and were also seen in the spinal cord. The majority of such false positive streamlines could, however, easily be recognized and edited to provide a good and uniform representation of the CST in three animals (JBG-3/4/5) (Fig. 4). Tractography parameters are summarized in Table 1.

4. Discussion

Our neuronal tracing data shows a consistent and relatively constant crossover of the vast majority of the Göttingen minipig corticospinal fibers suggesting a predominant right motor cortical control of the left body half. Additionally, the motor cortical axons project to the thalamus, brainstem, and rostral spinal cord wherein the general course of the CST was similar to what is known in humans and non-human primates (Gray et al., 2005). Likewise, we were able to demonstrate some axonal terminations on large neuronal cell bodies of the rostral cervical spinal cord ventral horn gray matter (Fig. 3F), although our study was not designed to quantify the degree of direct versus indirect CST influence on the lower motor neurons. We must, therefore, admit that insight on this important comparative feature (humans have a high degree of direct CST terminations (Gray et al., 2005; Nyberg-Hansen and Rinvik, 1963)) is not obtained by our study.

Another flaw of our study is that spinal cord tissue caudal to the mid-cervical levels was not retrieved. We are accordingly unable to demonstrate if the CST pattern demonstrated in the upper cervical spinal cord (Fig. 3C) continues unchanged all the way caudally through the spinal cord. Knowledge of this feature would be valuable, as the recent study by Leonard et al. (Leonard et al., 2017) indicates that the pig CST can only be seen in the cervical spinal cord. Contrary to this statement, fMRI (Fang et al., 2005) and muscle motor evoked potential (Tanaka et al., 2008) studies have suggested that the CST system may also influence the caudal spinal cord. The contrasting results may be explained by the degree of motor cortical tracing as some confusion exists on the exact location of the pig motor cortex and its somatotopic arrangement (Ariëns Kappers et al., 1967; Campbell, 1905; Saikali et al., 2010; Schmidt, 2015; Stephan, 1951). Thus, Jelsing et al. used cytoarchitecture and neuronal tracing to delineate the prefrontal cortex of Göttingen minipig (Jelsing et al., 2006). We value this paper highly, but the extension of the prefrontal areas is rather large compared to the motor areas. Thus, in a comparative aspect, non-primate mammals usually have less amount of prefrontal cortex compared to the amount of frontal motor cortex (Ariëns Kappers et al., 1967; Campbell, 1905). We have therefore reevaluated the cytoarchitecture of the Göttingen minipig telencephalon (Bjarkam et al., 2017a) claiming that the main part of the Jelsing et al. dorsofrontal prefrontal area should be designated motor cortex (primary + premotor cortex). It is noteworthy that Jelsing et al. (2006) use tracing to the thalamic MD nucleus as an prefrontal identifier, as we in the current study have tracing to this nucleus in our most rostral tracing injection in JBG-2, whereas the other injections are connected to the thalamic VA-VL regions. Hence, we find that these injections and their prominent contribution to the CST gives additional support to our delineation of the Göttingen minipig motor cortex, which in our material encompasses both the primary motor and the premotor area, as no clear cytoarchitectonic or connectional differences between these areas are visible in our data. Interestingly, the motor area lesioned by Palmieri et al., (Palmieri et al., 1986) in their seminal paper on the pig pyramidal tract is similar to our delineation (see their Fig. 2), although they electrophysiolocially identify a smaller motor area (more similar to the Jelsing delineation) in their Fig. 1. The difference between the Palmieri Figs. 1 and 2, might accordingly point to an electrophysiological difference between the pig primary motor and premotor areas not reflected in cytoarchitecture and thalamocortical connectivity. However, the mammal CST is formed by fibers not only originating in the primary motor cortex (30% in monkey) but also in the premotor (30% in monkey) and somatosensory (parietal) (40% in monkey) (Russell and DeMyer, 1961). Thus, injections in JBG-1/4 (probably primary motor) and injections in JBG-3/5 (probably premotor) would provide fibers to the CST as demonstrated in our study, whereas the injection in JBG-2 due to a different thalamocortical connectivity most be designated as prefrontal and accordingly not provide fibers to the CST.

Somatotopic arrangement of the piglet somatosensory cortex have been demonstrated by Craner and Ray (Craner and Ray, 1991a,b; Craner and Ray, 1986), just as the papers by Breazile et al. (Breazile

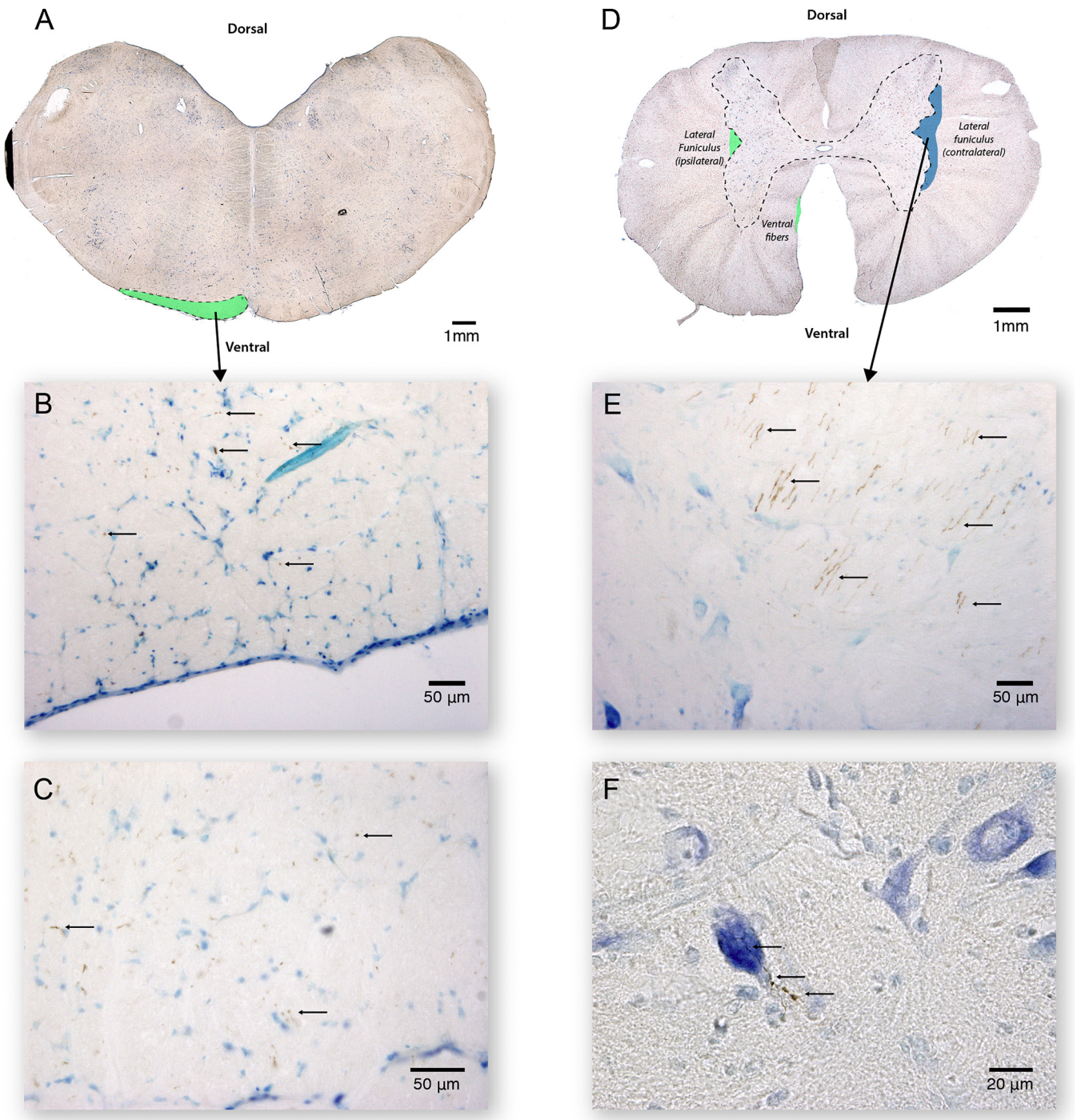

Fig. 3. Cross-sectional views of different magnification displaying the distribution of traced motor cortical axons (small arrows) in the most caudal brainstem (A–C) and most rostral cervical spinal cord (D–F) just below the pyramidal decussation in JBG-3. A and D are representative for the sections where stereological fiber quantification was made before and after crossing, where green areas contain ipsilateral fibers and blue areas contain contralateral fibers. B and C are displaying traced fibers in the brainstem pyramid, where C is in larger magnification. On E the crossed fibers in the contralateral lateral funiculus are seen in proximity to the ventral horn gray matter. F displays a traced motor cortical axon connecting to a large neuronal cell body located in the ventral horn of the gray matter in the rostral cervical spinal cord. Counterstaining with toluidine blue. (For interpretation of the references to color in this figure legend, the reader is referred to the web version of this article.)

et al., 1966) and Palmieri et al. (Palmieri et al., 1986) electrophysiologically demonstrate a somatotopic arrangement of the pig motor cortex into face, forelimb and hindlimb areas. Thus a pig homunculus" porculus" exist, but due to the rather large size of our injections and the variable and limited extent of the different motor areas, we did not beforehand aim to inject tracer in a specified somatomotor area. However, one would expect a pure hit in the face area to result in primary corticobulbar fibers, whereas a pure hit in the forelimb area primarily would result in corticospinal fibers to the cervical cord, which may be the case in the Leonard et al. study (Leonard et al., 2017), and a pure hit in the hind limb area to primarily result in corticospinal fibers into the thoracic-lumbar cord.

Thus, the classical view that the CST system of ungulates is not well developed (Lassek, 1942) and that motor cortical axons predominantly

Table 2
Summarization of the histological findings. The section topography was evaluated against a histological atlas. (†) Due to numerous freezing artifacts the cytostructural analysis of JBG 5 could not be made. (‡) Motor cortex, however, in a transition area. (VA) ventroanterior thalamic nucleus, (VL) ventrolateral thalamic nucleus, (MD) mediodorsal thalamic nucleus, (MC) motor cortex (primary + premotor), and (PFC) prefrontal cortex.

Animal No.	Predominant layers III and V	Large Pyramid Cells (Layer V)	MC consistent topography	Thalamic Nuclei	Pyramid fibers	Pyramid Decussation	Injected Cortical area
JBG-1	Yes	Yes	Yes‡	VA/VL	Yes	Crossing fibers	MC
JBG-2	Yes	No	No	MD	No	No crossing fibers	PFC
JBG-3	Yes	Yes	Yes	VL	Yes	Crossing fibers	MC
JBG-4	Yes	Yes	Yes	VL	Yes	Crossing fibers	MC
JBG-5	?†	Yes	Yes	VL	Yes	Crossing fibers	MC

project to bulbar nuclei and hence form a corticobulbar rather than corticospinal tract (Palmieri et al., 1986) has been questioned by both recent (Fang et al., 2005; Leonard et al., 2017; Tanaka et al., 2008) and our current study, since we found numerous axons in the cervical spinal cord of all animals traced from the motor cortex (Fig. 3). In three of four animals (JBG-3/4/5) the spinal axons represented over half of the fibers counted in the pyramid, pointing towards a higher cortical motor control of extremity and/or axial musculature. Keeping in mind, that corticospinal tracing is non-proximity tracing with a distant axonal tracer transport, the number of spinal projecting axons may even be greater since it is possible that not all axons transported the tracer all the way to the spinal cord before tracer fixation. The fact that the counted number of caudal "fibers after crossing" relative to more proximal "fibers before crossing" is increased in the three animals (JBG-3/4/5) with a longer survival time and hence longer tracer transport time could point towards this possibility.

The crossed corticospinal fibers were seen to predominantly descend in the lateral funiculus as in humans (Gray et al., 2005; Nyberg-Hansen and Rinvik, 1963). However, some crossed fibers also projected towards the dorsal funiculus and the dorsal horn of the spinal cord, which is more similar to the rodent spinal CST distribution (Brown, 1971; Watson et al., 2009). Contrarily to humans, the uncrossed corticospinal fibers were similarly seen to predominantly project ipsilateral in the lateral funiculus with few fibers projecting towards the dorsal horn. However, one animal (JBG-3) deviated with a group of such fibers being seen in the expected position in immediate proximity to the ventral median fissure, as is the case for the anterior corticospinal tract in humans (Gray et al., 2005; Nyberg-Hansen and Rinvik, 1963). Why such fibers were only found in this single animal could perhaps be explained by the motor cortical injection sites, which were somewhat slightly more laterally located in this animal.

A physiological segregation of distal versus axial motor function, which at least in humans is represented by the lateral and anterior corticospinal tract, respectively, could not be assessed in our study, but would require an electrophysiological approach. It is nonetheless plausible that an animal with a four-legged gait like the minipig could have a different degree of postural control, which could be manifested by a different corticospinal arrangement. To investigate possible fiber subpopulations and thickness differences between crossed and uncrossed fibers we did a microscopic measurement estimation of axon thickness of the uncrossed and crossed fibers residing in the lateral funiculi. These measurement data did not show significant differences, although there yet seemed to be a trend towards two axon subpopulations and towards the thickest of axons residing in the contralateral funiculus when comparing animals (data not shown).

The tractography data supported the neuronal tracing data showing an anatomically similar CST and provided a unique overview of white matter anatomy, which could not be obtained with neuronal tracing alone. However, the quantification of streamlines varied from the stereological quantification, which points towards the methodological differences, i.e. actual labeled axons versus resembling streamlines. This is likely due to several factors including the relatively long CST path length, as a relation exists between the path length and the number of false positives and negatives, as well as path-length dependency confounds in probabilistic tractography (Donahue et al., 2016; Liptrot et al., 2014). Moreover, others have argued that tractography used for trajectories crossing gray matter areas may exacerbate inherent challenges in this method (Donahue et al., 2016), which could be another explanation for the deviating results. Additionally, the streamlines cannot traverse the low anisotropic spinal gray matter and hence not follow the true anatomical course of the CST, which causes streamlines to either terminate at the crossing level or proceed in the highly anisotropic anteromedial spinal cord white matter affecting the crossover ratio. With the neuroanatomical knowledge from the neuronal tracing data, it is therefore not possible to quantify the CST using tractography, which represents a method limitation.

As described in previous studies (Tournier et al., 2012), we also observed well known challenges in complex white matter regions consisting of crossing fibers, e.g. the centrum semiovale and areas in the brainstem, leading to smaller fractions of false positive streamlines deviating from the general course of the CST. The availability of neuronal tracing data to confirm such false positives is, however, still representing another limitation of this otherwise refined method, which is of utmost importance to consider when implementing tractography for clinical neurosurgical guidance.

The initial CST tractography made before applying the ICE-T region-growing method showed an unreliable ratio of generated versus selected streamlines (data not shown), which was indicative of the previously described path-length dependency confounds in probabilistic tractography (Liptrot et al., 2014), but such confounds were avoided

Table 3
Overview of fiber quantification before crossing and after crossing, where the latter is subdivided in columns of the ipsilateral and contralateral spinal half, respectively. The 'crossed fibers' column is the ratio of ipsilateral versus contralateral fiber count. The injection volume is estimated by the Cavalieri method and is noted with respective observed coefficient of error (OCE). Ratios of fibers per injection volume are seen to the right, both before and after crossover. (†) Unfortunately, these sections were not surface stained and orientation is hence determined through more cranial and caudal sections with surface staining.

Animal no.	Fibers before n	Fibers after n	Ipsi-lateral n	Contra-lateral n	Crossed fibers %	Injection volume mm3 (OCE)	Ratio fibers per volume before cross	Ratio fibers per volume after cross
JBG-1	496	136	12	124	91,2	17,52 (0,075)	28,3	7,8
JBG-3	1120	632	120	512	81,0	39,98 (0,047)	28,0	15,8
JBG-4	640	408	36	372	91,2	26,67 (0,069)	24,0	15,3
JBG-5†	1728	904	64	840	92,9	23,9 (0,053)	72,3	37,8

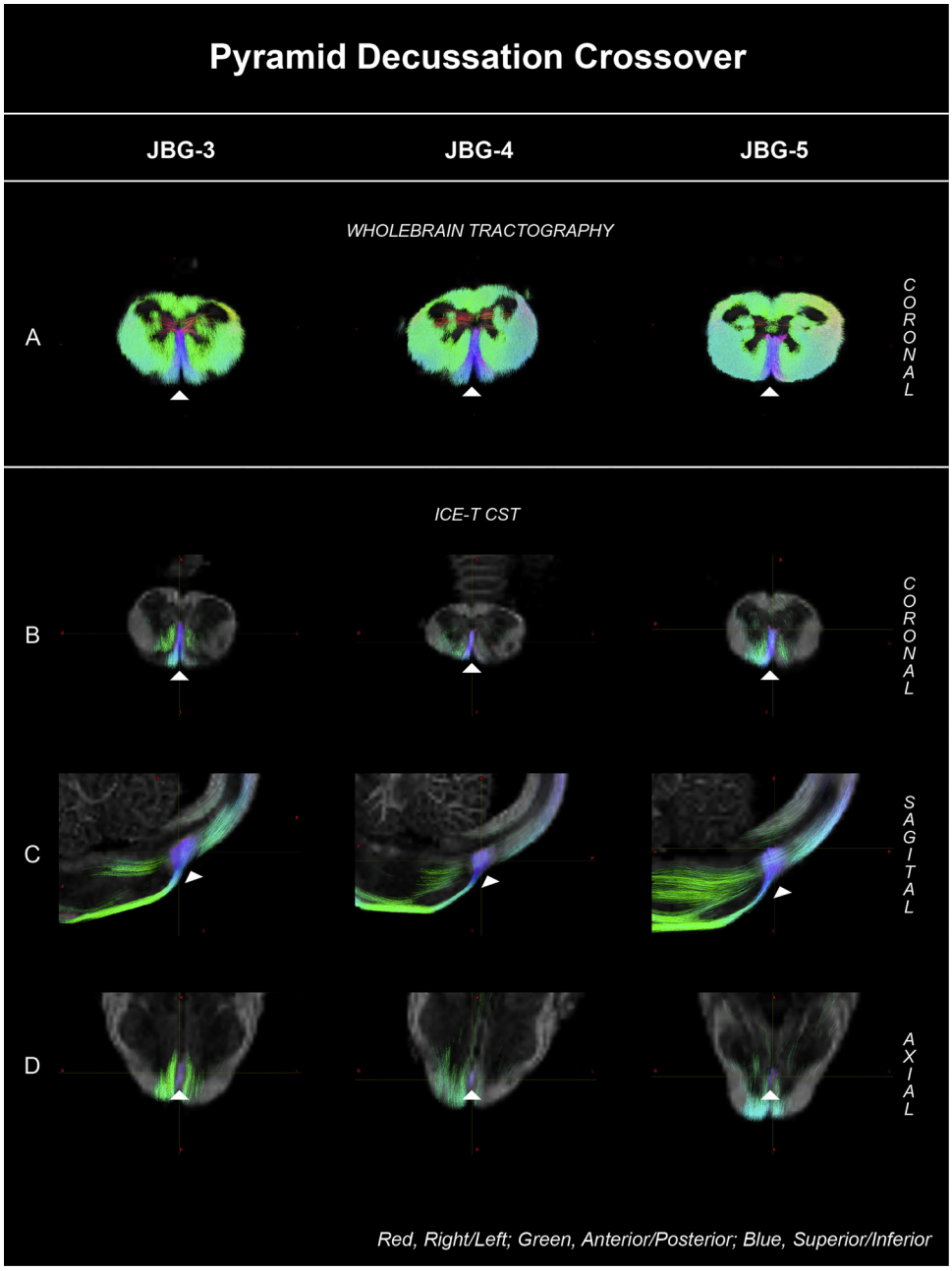

Fig. 4. "Whole brain" and ICE-T CST tractography from animals JBG-3/4/5. Row A is coronal and thus cross-sectional views of the whole brain tractography displaying the pyramid decussation with crossing fibers seen in blue/purple (arrowheads). Rows B–D are the ICE-T CST shown in orthogonal view. Focus is set on the pyramid decussation, from where the same crossing fibers seen in blue (arrowheads) as seen in row A are hence part of the corticospinal tract. (For interpretation of the references to color in this figure legend, the reader is referred to the web version of this article.)

Table 4
Quantification of streamlines using MRtrix 3 'tckedit'. The varying crossover percentage between the uncrossed streamlines in the "ipsilateral" spinal half column and the crossed streamlines in the "contralateral" spinal half column is displayed in the right column.

Animal No.	Streamlines Before	Streamlines Ipsilateral	Streamlines Contralateral	Crossed streamlines %
JBG-3	131	38	7	15,56
JBG-4	82	10	4	28,57
JBG-5	362	36	2	5,26

using this approach. The fact that the CST is traversing more complex white matter areas may further have contributed to this ratio. As mentioned, streamlines terminated in or unreliably traversed the less anisotropic spinal gray matter, which especially for the ICE-T approach resulted in false positives in the spinal cord. Accordingly, this shows a method limitation since tractography was not able to display that the majority of CST fibers was traversing the spinal gray matter. The CST from its origin in the motor cortex to the crossing of fibers at the pyramid decussation could, however, be visualized with close resemblance to neuronal tracing data and with a limited and explainable number of false positives, which for most part was readily recognizable and therefore easily edited with the underlying knowledge from the tracing data. Moreover, the CST could be consistently visualized bilaterally and across animals. Tractography, therefore, yet holds much promise and is

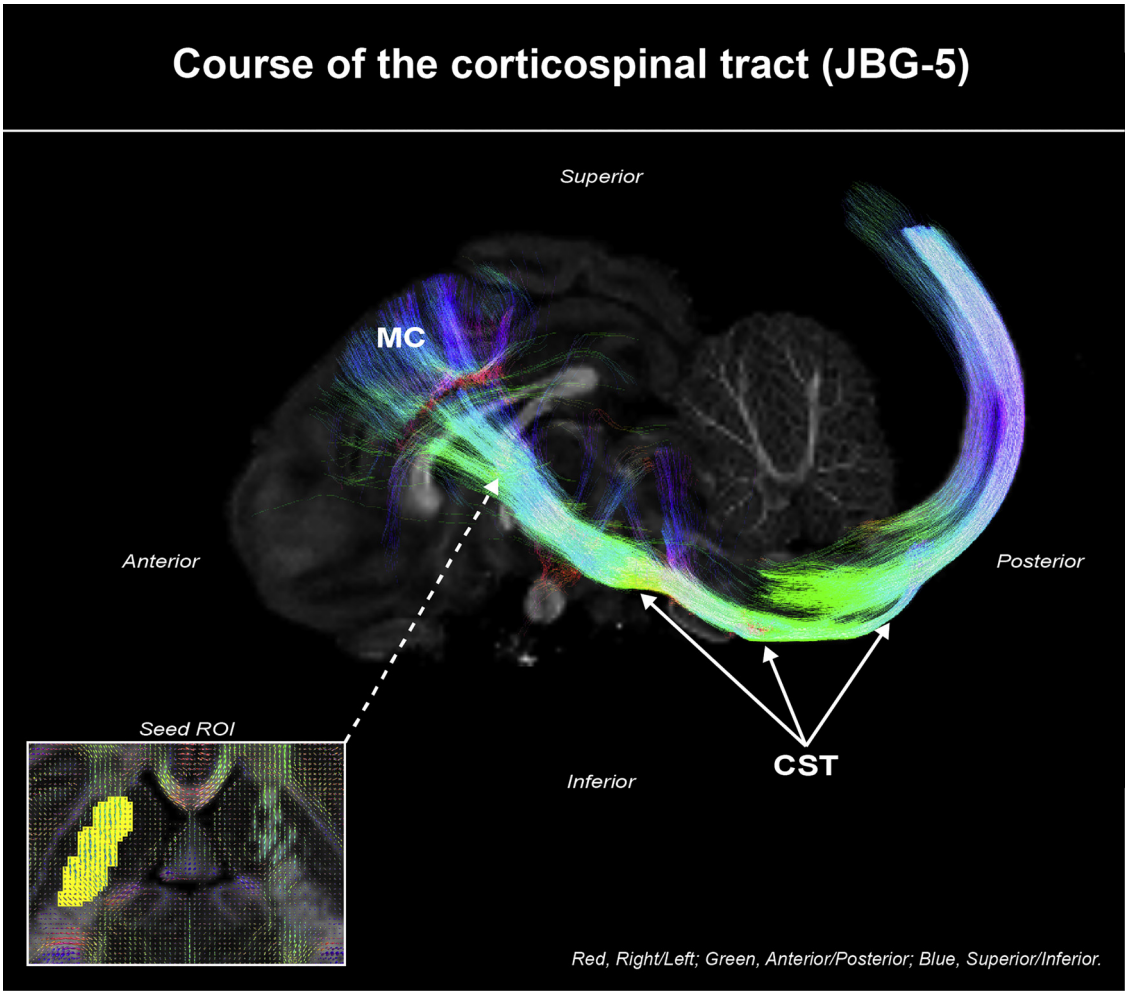

Fig. 5. Sagittal view of the corticospinal tract of JBG-5 made using ICE-T tractography. Streamlines are not "cropped to slab" in order to provide a better overview. The tract of JBG-5 is representative of the other animals and closely resembles the neuronal tracing data, but provides a better overview. From its origin at the motor cortex (MC), the corticospinal tract (CST) traverses the internal capsule and brainstem before descending the spinal cord, which is folded above the cerebellum. The bottom left window display the ROI in the internal capsule (yellow area) used for streamline seeding and also FOD glyphs. (For interpretation of the references to color in this figure legend, the reader is referred to the web version of this article.)

able to provide an excellent white matter anatomical overview, which may be valuable, e.g. for generating future neuroanatomical hypotheses.

5. Conclusion

Benefitting from the combined method strengths of neuronal tracing, tractography and unbiased stereology, our study provides a detailed description of the encephalic part of the Göttingen minipig corticospinal system including the degree of decussation and spinal location of the CST system in the upper cervical spinal cord. The provided data indicate that the porcine CST system is more developed and lateralized than previous believed, supporting further advancement of this large animal model for translational research on CNS diseases with prominent motor dysfunction.

Conflict of interest

We wish to confirm that there are no known conflicts of interest associated with this publication and there has been no significant financial support for this work that could have influenced its outcome.

Acknowledgments

We acknowledge the laboratory assistance by Ms. Trine W. Mikkelsen, the assistance and administration by Ms. Lise Moberg Fitting and Ms. Anne Sofie Møller Andersen, and the help of Påskehøjgaard animal facility. Thanks to the Novo Nordisk Foundation, the Jascha Foundation, "Fonden for Neurologisk Forskning", and "Simon Fougner Hartmanns Familiefond" for funding.

References

Anaya Garcia, M.S., Hernandez Anaya, J.S., Marrufo Melendez, O., Velazquez Ramirez, J.L., Palacios Aguiar, R., 2015. In vivo study of cerebral white matter in the dog using diffusion tensor tractography. Vet. Radiol. Ultrasound 56, 188–195.

Ariëns Kappers, C.U., Huber, G.C., Crosby, E.C., 1967. The Comparative Anatomy of the Nervous System of Vertebrates, Including Man. Hafner Publishing Company, New York.

Behrens, T.E., Berg, H.J., Jbabdi, S., Rushworth, M.F., Woolrich, M.W., 2007. Probabilistic diffusion tractography with multiple fibre orientations: what can we gain? Neuroimage 34, 144–155.

Bjarkam, C.R., Pedersen, M., Sorensen, J.C., 2001. New strategies for embedding, orientation and sectioning of small brain specimens enable direct correlation to MR-images, brain atlases, or use of unbiased stereology. J. Neurosci. Methods 108, 153–159.

Bjarkam, C.R., Cancian, G., Larsen, M., Rosendahl, F., Ettrup, K.S., Zeidler, D., Blankholm, A.D., Ostergaard, L., Sunde, N., Sorensen, J.C., 2004. A MRI-compatible stereotaxic localizer box enables high-precision stereotaxic procedures in pigs. J. Neurosci. Methods 139, 293–298.

Bjarkam, C.R., Nielsen, M.S., Glud, A.N., Rosendal, F., Mogensen, P., Bender, D., Doudet, D., Moller, A., Sorensen, J.C., 2008. Neuromodulation in a minipig MPTP model of Parkinson disease. Br. J. Neurosurg. 22 (Suppl. 1), S9–12.
Bjarkam, C.R., Cancian, G., Glud, A.N., Ettrup, K.S., Jorgensen, R.L., Sorensen, J.C., 2009. MRI-guided stereotaxic targeting in pigs based on a stereotaxic localizer box fitted with an isocentric frame and use of SurgiPlan computer-planning software. J. Neurosci. Methods 183, 119–126.
Bjarkam, C.R., Glud, A.N., Orlowski, D., Sorensen, J.C., Palomero-Gallagher, N., 2017a. The telencephalon of the Gottingen minipig, cytoarchitecture and cortical surface anatomy. Brain Struct. Funct. 222 (5), 2093–2114.
Bjarkam, C.R., Orlowski, D., Tvilling, L., Bech, J., Glud, A.N., Sorensen, J.H., 2017b. Exposure of the pig CNS for histological analysis: a manual for decapitation, skull opening, and brain removal. J. Vis. Exp. e55511, 45–48.
Brandt, H.M., Apkarian, A.V., 1992. Biotin-dextran: a sensitive anterograde tracer for neuroanatomic studies in rat and monkey. J. Neurosci. Methods 45, 35–40.
Breazile, J.E., Swafford, B.C., Thompson, W.D., 1966. Study of the motor cortex of the domestic pig. Am. J. Vet. Res. 27, 1369–1373.
Brown, L.T., 1971. Projections and termination of the corticospinal tract in rodents. Exp. Brain Res. 13, 432–450.
Calabrese, E., Badea, A., Cofer, G., Qi, Y., Johnson, G.A., 2015. A Diffusion MRI tractography connectome of the mouse brain and comparison with neuronal tracer data. Cereb. Cortex 25, 4628–4637.
Campbell, A., 1905. Histological Studies on the Localisation of Cerebral Function. Cambridge University Press.
Christensen, A.B., Sorensen, J.C.H., Ettrup, K.S., Orlowski, D., Bjarkam, C.R., 2018. Pirouetting pigs: a large non-primate animal model based on unilateral 6-hydroxydopamine lesioning of the nigrostriatal pathway. Brain Res. Bull. 139, 167–173.
Craner, S.L., Ray, R.H., 1986. Topographic organization of somatosensory cortices SI and SII of the neonatal pig. Physiologist 29, 120.
Craner, S.L., Ray, R.H., 1991a. Somatosensory cortex of the neonatal pig: I. Topographic organization of the primary somatosensory cortex (SI). J. Comp. Neurol. 306, 24–38.
Craner, S.L., Ray, R.H., 1991b. Somatosensory cortex of the neonatal pig: II. Topographic organization of the secondary somatosensory cortex (SII). J. Comp. Neurol. 306, 39–48.
Cumming, P., Danielsen, E.H., Vafaee, M., Falborg, L., Steffensen, E., Sorensen, J.C., Gillings, N., Bender, D., Marthi, K., Andersen, F., Munk, O., Smith, D., Moller, A., Gjedde, A., 2001. Normalization of markers for dopamine innervation in striatum of MPTP-lesioned miniature pigs with intrastriatal grafts. Acta Neurol. Scand. 103, 309–315.
Dolezalova, D., Hruska-Plochan, M., Bjarkam, C.R., Sorensen, J.C., Cunningham, M., Weingarten, D., Ciacci, J.D., Juhas, S., Juhasova, J., Motlik, J., Hefferan, M.P., Hazel, T., Johe, K., Carromeu, C., Muotri, A., Bui, J., Strnadel, J., Marsala, M., 2014. Pig models of neurodegenerative disorders: utilization in cell replacement-based preclinical safety and efficacy studies. J. Comp. Neurol. 522, 2784–2801.
Donahue, C.J., Sotiropoulos, S.N., Jbabdi, S., Hernandez-Fernandez, M., Behrens, T.E., Dyrby, T.B., Coalson, T., Kennedy, H., Knoblauch, K., Van Essen, D.C., Glasser, M.F., 2016. Using diffusion tractography to predict cortical connection strength and distance: a quantitative comparison with tracers in the monkey. J. Neurosci. 36, 6758–6770.
Dyrby, T.B., Sogaard, L.V., Parker, G.J., Alexander, D.C., Lind, N.M., Baare, W.F., Hay-Schmidt, A., Eriksen, N., Pakkenberg, B., Paulson, O.B., Jelsing, J., 2007. Validation of in vitro probabilistic tractography. Neuroimage 37, 1267–1277.
Dyrby, T.B., Baare, W.F., Alexander, D.C., Jelsing, J., Garde, E., Sogaard, L.V., 2011. An ex vivo imaging pipeline for producing high-quality and high-resolution diffusion-weighted imaging datasets. Hum. Brain Mapp. 32, 544–563.
Ettrup, K.S., Glud, A.N., Orlowski, D., Fitting, L.M., Meier, K., Soerensen, J.C., Bjarkam, C.R., Alstrup, A.K., 2011. Basic surgical techniques in the Gottingen minipig: intubation, bladder catheterization, femoral vessel catheterization, and transcardial perfusion. J. Vis. Exp.(52).
Fang, M., Lorke, D.E., Li, J., Gong, X., Yew, J.C., Yew, D.T., 2005. Postnatal changes in functional activities of the pig's brain: a combined functional magnetic resonance imaging and immunohistochemical study. Neurosignals 14, 222–233.
Fang, X., Mou, Y., Huang, Z., Li, Y., Han, L., Zhang, Y., Feng, Y., Chen, Y., Jiang, X., Zhao, W., Sun, X., Xiong, Z., Yang, L., Liu, H., Fan, D., Mao, L., Ren, L., Liu, C., Wang, J., Li, K., Wang, G., Yang, S., Lai, L., Zhang, G., Li, Y., Wang, J., Bolund, L., Yang, H., Wang, J., Feng, S., Li, S., Du, Y., 2012. The sequence and analysis of a Chinese pig genome. Gigascience 1, 16.
FSL webpage, Last Accessed (4 December 2017). (http://fsl.fmrib.ox.ac.uk/fsl/fslwiki/FSL).
Glud, A.N., Hedegaard, C., Nielsen, M.S., Sorensen, J.C., Bendixen, C., Jensen, P.H., Larsen, K., Bjarkam, C.R., 2010. Direct gene transfer in the Gottingen minipig CNS using stereotaxic lentiviral microinjections. Acta Neurobiol. Exp. (Wars) 70, 308–315.
Glud, A.N., Hedegaard, C., Nielsen, M.S., Sorensen, J.C., Bendixen, C., Jensen, P.H., Mogensen, P.H., Larsen, K., Bjarkam, C.R., 2011. Direct MRI-guided stereotaxic viral mediated gene transfer of alpha-synuclein in the Gottingen minipig CNS. Acta Neurobiol. Exp. (Wars) 71, 508–518.
Glud, A.N., Bech, J., Tvilling, L., Zaer, H., Orlowski, D., Fitting, L.M., Ziedler, D., Geneser, M., Sangill, R., Alstrup, A.K.O., Bjarkam, C.R., Sorensen, J.C.H., 2017. A fiducial skull marker for precise MRI-based stereotaxic surgery in large animal models. J. Neurosci. Methods 285, 45–48.
Gray, H., Standring, S., Ellis, H., Berkovitz, B.K.B., 2005. Gray's Anatomy – The Anatomical Basis of Clinical Practice, thirty-ninth edition. Elsevier Churchill Livingstone.
Han, X., Lv, G., Wu, H., Ji, D., Sun, Z., Li, Y., Tang, L., 2012. Biotinylated dextran amine anterograde tracing of the canine corticospinal tract. Neural Regen. Res. 7, 805–809.
Jelsing, J., Hay-Schmidt, A., Dyrby, T., Hemmingsen, R., Uylings, H.B., Pakkenberg, B., 2006. The prefrontal cortex in the Gottingen minipig brain defined by neural projection criteria and cytoarchitecture. Brain Res. Bull. 70, 322–336.
Jenkinson, M., Beckmann, C.F., Behrens, T.E., Woolrich, M.W., Smith, S.M., 2012. FSL. Neuroimage 62, 782–790.
Jones, D.K., 2004. The effect of gradient sampling schemes on measures derived from diffusion tensor MRI: a Monte Carlo study. Magn. Reson. Med. 51, 807–815.
Lassek, A.M., 1942. The pyramidal tract. A fiber and numerical analysis in a series of non-digital mammals (ungulates). J. Comp. Neurol. 77, 399–404.
Lazarov, N.E., 2013. Neuroanatomical tract-tracing using biotinylated dextran amine. Methods Mol. Biol. 1018, 323–334.
Leonard, A.V., Menendez, J.Y., Pat, B.M., Hadley, M.N., Floyd, C.L., 2017. Localization of the corticospinal tract within the porcine spinal cord: implications for experimental modeling of traumatic spinal cord injury. Neurosci. Lett. 648, 1–7.
Lind, N.M., Moustgaard, A., Jelsing, J., Vajta, G., Cumming, P., Hansen, A.K., 2007. The use of pigs in neuroscience: modeling brain disorders. Neurosci. Biobehav. Rev. 31, 728–751.
Liptrot, M.G., Sidaros, K., Dyrby, T.B., 2014. Addressing the path-length-dependency confound in white matter tract segmentation. PLoS One 9, e96247.
MRtrix 3 webpage, Last Accessed (4 December 2017). (http://www.mrtrix.org).
Nance, D.M., Burns, J., 1990. Fluorescent dextrans as sensitive anterograde neuroanatomical tracers: applications and pitfalls. Brain Res. Bull. 25, 139–145.
Nielsen, M.S., Glud, A.N., Moller, A., Mogensen, P., Bender, D., Sorensen, J.C., Doudet, D., Bjarkam, C.R., 2016. Continuous MPTP intoxication in the Gottingen minipig results in chronic parkinsonian deficits. Acta Neurobiol. Exp. (Wars) 76, 199–211.
Nyberg-Hansen, R., Rinvik, E., 1963. Some comments on the pyramidal tract, with special reference to its individual variations in man. Acta Neurol. Scand. 39, 1–30.
Palmieri, G., Farina, V., Panu, R., Asole, A., Sanna, L., De Riu, P.L., Gabbi, C., 1986. Course and termination of the pyramidal tract in the pig. Arch. Anat. Microsc. Morphol. Exp. 75, 167–176.
Reiner, A., Veenman, C.L., Medina, L., Jiao, Y., Del Mar, N., Honig, M.G., 2000. Pathway tracing using biotinylated dextran amines. J. Neurosci. Methods 103, 23–37.
Russell, J.R., DeMyer, W., 1961. The quantitative cortical origin of pyramidal axons of Macaca rhesus with some remarks on slow rate of axolysis. Neurology 11, 96.
Saikali, S., Meurice, P., Sauleau, P., Eliat, P.A., Bellaud, P., Randuineau, G., Verin, M., Malbert, C.H., 2010. A three-dimensional digital segmented and deformable brain atlas of the domestic pig. J. Neurosci. Methods 192, 102–109.
Schmidt, V., 2015. Comparative Anatomy of the Pig Brain: an Integrative Magnetic Resonance Imaging (MRI) Study of the Porcine Brain With Special Emphasis on the External Morphology of the Cerebral Cortex. Universitätsbibliothek, Gieflen.
Schubert, R., Frank, F., Nagelmann, N., Liebsch, L., Schuldenzucker, V., Schramke, S., Wirsig, M., Johnson, H., Kim, E.Y., Ott, S., Holzner, E., Demokritov, S.O., Motlik, J., Faber, C., Reilmann, R., 2016. Neuroimaging of a minipig model of Huntington's disease: feasibility of volumetric, diffusion-weighted and spectroscopic assessments. J. Neurosci. Methods 265, 46–55.
Solnitzky, O., 1938. The thalamic nuclei of Sus scrofa. J. Comp. Neurol. 69, 121–169.
Stephan, H., 1951. Vergleichende untersuchungen über den feinbau des hirnes von wild- und haustieren. Zoologisches Jahrbuch, Abteilung für Anatomie und Ontogenie 71, 487–586.
Tanaka, Y., Imai, H., Konno, K., Miyagishima, T., Kubota, C., Puentes, S., Aoki, T., Hata, H., Takata, K., Yoshimoto, Y., Saito, N., 2008. Experimental model of lacunar infarction in the gyrencephalic brain of the miniature pig: neurological assessment and histological, immunohistochemical, and physiological evaluation of dynamic corticospinal tract deformation. Stroke 39, 205–212.
Tournier, J.D., Calamante, F., Gadian, D.G., Connelly, A., 2004. Direct estimation of the fiber orientation density function from diffusion-weighted MRI data using spherical deconvolution. Neuroimage 23, 1176–1185.
Tournier, J.D., Calamante, F., Connelly, A., 2007. Robust determination of the fibre orientation distribution in diffusion MRI: non-negativity constrained super-resolved spherical deconvolution. Neuroimage 35, 1459–1472.
Tournier, J.D., Calamante, F., Connelly, A., 2010. Improved probabilistic streamlines tractography by 2nd order integration over fibre orientation distributions. Proceedings of the International Society for Magnetic Resonance in Medicine. pp. 1670.
Tournier, J.D., Calamante, F., Connelly, A., 2012. MRtrix: Diffusion tractography in crossing fiber regions. Int. J. Imaging Syst. Technol. 22, 53–66.
Veenman, C.L., Reiner, A., Honig, M.G., 1992. Biotinylated dextran amine as an anterograde tracer for single- and double-labeling studies. J. Neurosci. Methods 41, 239–254.
Vercelli, A., Repici, M., Garbossa, D., Grimaldi, A., 2000. Recent techniques for tracing pathways in the central nervous system of developing and adult mammals. Brain Res. Bull. 51, 11–28.
Watson, C., Paxinos, G., Kayalioglu, G., 2009. Elsevier Ltd, San Diego. The Spinal Cord: A Christopher and Dana Reeve Foundation Text and Atlas.
West, M.J., 2012a. Estimating object number in biological structures. Cold Spring Harb. Protoc. 2012, 1049–1066.
West, M.J., 2012b. Estimating volume in biological structures. Cold Spring Harb. Protoc. 2012, 1129–1139.